

## Accepted Manuscript

Research paper

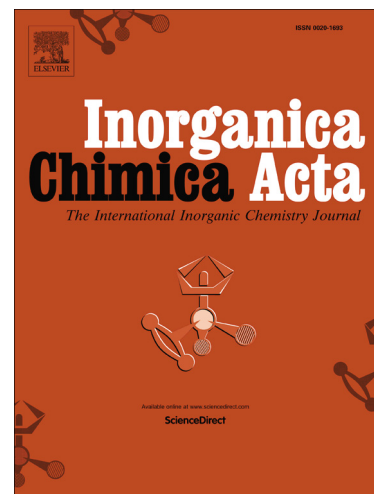
Ultrasonic assisted synthesis, crystallographic, spectroscopic studies and biological activity of three new Zn(II), Co(II) and Ni(II) thiosemicarbazone complexes as precursors for nano-metal oxides

Zahra Piri, Zeinab Moradi-Shoeili, Abdeljalil Assoud

PII: S0020-1693(18)30135-X  
DOI: <https://doi.org/10.1016/j.ica.2018.09.054>  
Reference: ICA 18512

To appear in: *Inorganica Chimica Acta*

Received Date: 25 January 2018  
Revised Date: 29 August 2018  
Accepted Date: 20 September 2018



Please cite this article as: Z. Piri, Z. Moradi-Shoeili, A. Assoud, Ultrasonic assisted synthesis, crystallographic, spectroscopic studies and biological activity of three new Zn(II), Co(II) and Ni(II) thiosemicarbazone complexes as precursors for nano-metal oxides, *Inorganica Chimica Acta* (2018), doi: <https://doi.org/10.1016/j.ica.2018.09.054>

This is a PDF file of an unedited manuscript that has been accepted for publication. As a service to our customers we are providing this early version of the manuscript. The manuscript will undergo copyediting, typesetting, and review of the resulting proof before it is published in its final form. Please note that during the production process errors may be discovered which could affect the content, and all legal disclaimers that apply to the journal pertain.

**Ultrasonic assisted synthesis, crystallographic, spectroscopic studies and biological activity of three new Zn(II), Co(II) and Ni(II) thiosemicarbazone complexes as precursors for nano-metal oxides**

Zahra Piri<sup>1</sup>, Zeinab Moradi-Shoeili,<sup>\*1</sup> Abdeljalil Assoud<sup>2</sup>

<sup>1</sup> *Department of Chemistry, Faculty of Sciences, University of Guilan, P.O. Box 41335-1914, Rasht, Iran*

<sup>2</sup> *Department of Chemistry, University of Waterloo, Waterloo, Ontario, N2L 3G1 Canada*

**Abstract**

Using ultrasonic irradiations, three new complexes of type  $[\text{ZnL}_2].\text{CH}_3\text{CN}$ ,  $[\text{NiLCl}]$  and  $[\text{CoL}_2]$  (where L is 2-acetylpyridine -4N-p-chlorophenylthiosemicarbazone ligand) have been prepared and investigated using various spectroscopic methods. Crystal structures of  $\text{ZnL}_2$  and  $\text{NiLCl}$  complexes displayed distorted octahedral and square-planar coordination geometry around the central metal, respectively. The UV-Visible and mass spectroscopic analysis revealed 1:2 (metal:ligand) stoichiometry for Co(II) complex. The synthesized complexes have been used as precursors for preparing their corresponding nano-sized metal oxides via thermal decomposition. The nanostructures of metal oxides were characterized by scanning electron microscope (SEM), energy dispersive X-ray (EDX), X-ray diffraction (XRD) and Fourier transform infrared (FT-IR). The *in vitro* antibacterial activity of thiosemicarbazone complexes and their corresponding nano-sized metal oxides were studied against a series of gram positive and gram negative bacteria, using the zone inhibition methods. While  $\text{NiLCl}$  complex was shown to possess more

---

\* Corresponding author. Tel.: +98 13 33333262; fax: +98 13 33320066  
*E-mail address:* zmoradi@guilan.ac.ir (Z. Moradi-Shoeili)

antimicrobial activity than its nano-sized metal oxide, the prepared nano-sized zinc and cobalt oxides have shown the highest activity.

**Keywords:** Sonochemical synthesis; Thiosemicarbazone; Transition metal complexes; nano-sized metal oxide; Antibacterial.

## 1. Introduction

By combination of hydrazine group with aldehydes or ketones, one of the important classes of Schiff base ligands, namely thiosemicarbazones were generated and have found to possess various biological and pharmaceutical activities. Pyridine-2-carbaldehyde thiosemicarbazone was the first reported heterocyclic compound with carcinostatic properties [1]. Further investigations revealed that thiosemicarbazones possessing N-heterocycles such as pyridine in their structures usually show significant biological activities in vitro and in vivo [2]. Interestingly, the study of the structure–activity relationship of thiosemicarbazone derivatives have shown that their biological activity can be affected by introducing structural variation in N-heterocyclic ring and terminal amino substitution [3]. Due to high delocalized  $\pi$ -electrons throughout the moiety, thiosemicarbazones usually form a planar structure and also show good versatility as ligands [4]. The deprotonated thiosemicarbazone ligands represented by two tautomeric keto-enol forms and usually coordinate to metal ions through sulfur (S) and hydrazinic N donor atoms which are believed to possess the pharmaceutical activity of the original molecule [5]. The other potential donor atoms on the thiosemicarbazone backbone can further increase the coordination possibilities of these chelating ligands.

Moreover, the metal chelation ability of thiosemicarbazone ligands can cause drastic changes in their biological properties [6]. Some experimental evidences supported that the metal complexes

of thiosemicarbazones usually show a higher bioactivity and lower side effects compared to the free ligands [7, 8]. Previous studies have illustrated that the lipophilicity, which controls the rate of entry of molecules into the cell, may be enhanced by complexation [9]. However, the mechanisms involved in the pharmaceutical activity of thiosemicarbazones and their complexes are far from clear [10] and the direct relationship between the complexation and therapeutic strategy are still intriguing and controversial.

In recent years, the growth of drug-resistance pathogens due to the biological and morphological modifications has led the great demand of novel drugs with enhanced, targeted activity [11]. Further to this, metallo-drugs can act as effective antimicrobial and antibacterial agents in the mechanisms differing from organic drugs [12]. In this context, the synthesis of different thiosemicarbazone ligands and their complexes particularly with the first row of transition metals have received considerable attention due to the wide range of applications in pharmacological fields of both ligand and complexes [13, 14].

Metal oxide nanoparticles have been widely studied for their potent antibacterial activities [15]. Previous results have shown that metal oxide nanoparticles exhibit bactericidal properties through reactive oxygen species (ROS) generation effected by their physical structure and metal ion release [16]. Between different methodologies used for preparation of metal oxide nanomaterials, such as sol-gel, solid-state synthesis, and microemulsion methods, [17, 18], thermal decomposition process has been attracted much attention [19-21]. This technique involves the heat decomposition of the coordination or organometallic compounds, as precursors, to form the nano-crystalline products [22]. The thermal decomposition technique has its advantages; it is easy to be carried out under normal atmosphere, does not involved complicated processes, special equipment, or inert atmosphere and short period of time in comparison to solid

state reactions (long reaction time), sol-gel (difficult to control), and also it offers high purity and yield of the products. Therefore, the thermal decomposition technique has been explored as a convenient and efficient pathway for the preparation of nano-scale metal oxides [23, 24].

Keeping in mind the above observations and in continuation of our work in the area of thiosemicarbazone complexes [25, 26] we recently reported the antibacterial and antioxidant study of bioactive 2-acetylpyridine-4N-*p*-chlorophenylthiosemicarbazone ligand and the corresponding copper (II) complex [Cu(L)Cl]. Results have shown that the involvement of pyridine cycle in the ligand backbone enhanced the antibacterial activity of the thiosemicarbazone ligand in comparison with its thiosemicarbazide precursor. Moreover, we have established that copper complex [CuLCl] has more antibacterial activity than the ligand alone, in most cases [27]. These results encouraged us to further investigate the antibacterial properties of other transition metal complexes of this thiosemicarbazone ligand. Therefore, here we describe the synthesis of three new Zn(II), Ni(II) and Co(II) complexes with 2-acetylpyridine-4N-*p*-chlorophenylthiosemicarbazone ligand using ultrasonic irradiations, which significantly reduced the synthetic time and temperature. The analytical and physico-chemical analysis confirmed the composition and the structure of the newly synthesized complexes. Moreover, the corresponding nano-sized metal oxide derivatives were prepared by thermal decomposition method and their nanostructures were characterized by different spectroscopic methods. In addition, the *in vitro* antibacterial activity of thiosemicarbazone complexes and their metal oxides have been screened against a series of gram positive and gram negative bacteria, using the zone inhibition methods. Investigation of various organometallic and nanostructure compounds and screening the results of their antibacterial activity could be helpful in identifying

the effect of metal cations and complex structure on their mechanism and thereby encouraging further research in designing promising novel compounds with drug-like properties.

## 2. Experimental

### 2.1. Chemical reagents, Instrumentation and physical measurements

The chemicals for the synthesis were commercial products of the highest available purity and were used without further purification. 2-acetylpyridine-4N-p-chlorophenylthiosemicarbazone ligand has been synthesized as described previously [27]. Infrared spectra ( $4000\text{--}400\text{ cm}^{-1}$ ) of solid samples were taken as 1% dispersion in KBr pellets using a Shimadzu IR-470 FT-IR spectrophotometer. Elemental analysis (C, H, N) data were performed on a Perkin Elmer 2400 CHNS/O elemental analyzer. NMR spectra were obtained on a Bruker 500-DRX Avance spectrometer in  $\text{DMSO-d}_6$ . Electron ionization mass spectrometric (EI-MS) measurements were carried out with an Agilent HP 5973 spectrometer. UV-vis spectra were recorded by a Photonix Ar2017 UV-vis spectrophotometer. The scanning electron microscopy (SEM) images were taken on a KYKY-EM3200 scanning electron microscope. Powder X-ray diffraction (PXRD) data were collected with a Philips pw 1830 diffractometer (Cu-K $\alpha$  X-radiation,  $\lambda = 1.54\text{ \AA}$ ). The elemental analysis was recorded with an energy dispersive X-ray (EDX) analyzer, MIRA3 FEG-SEM series.

### 2.2. Sonochemical Synthesis of Zn(II), Co(II) and Ni(II) thiosemicarbazone complexes

A solution of the ligand HL (0.100 g, 1mmol), which was dissolved in 5 mL of ethanol was added drop wise to a solution of different metal salt ( $\text{Zn}(\text{NO}_3)_2 \cdot 6\text{H}_2\text{O}$  (0.076 g, 1mmol),  $\text{Co}(\text{NO}_3)_2 \cdot 6\text{H}_2\text{O}$  (0.096 g, 1mmol) and/or  $\text{NiCl}_2 \cdot 6\text{H}_2\text{O}$  (0.078 g, 1mmol)] in 5 mL ethanol while

it was positioned in a large-density ultrasonic probe, operating at 37 kHz with a maximum force output of 320 W. The reaction mixture was then sonicated for 30 min. The products was filtered off, washed with cold ethanol and diethyl ether and dried in air. The crystals of Zn and Ni complex were obtained by slow diffusion of acetonitrile in DMF solution of the compound.

Anal. Calc for  $\text{ZnL}_2 \cdot \text{CH}_3\text{CN}$  ( $\text{C}_{30}\text{H}_{27}\text{Cl}_2\text{N}_9\text{S}_2\text{Zn}$ ): C, 50.46; H, 3.81; N, 17.66;. Found: C, 51.03; H, 3.16; N, 17.15.

Anal. Calc for  $[\text{CoL}_2]$  ( $\text{C}_{28}\text{H}_{24}\text{Cl}_2\text{N}_8\text{S}_2\text{Co}$ ): C, 50.46; H, 3.63; N, 16.81;. Found: C, 50.82; H, 4.07; N, 16.68.

Anal. Calc for  $\text{NiLCl}$  ( $\text{C}_{14}\text{H}_{12}\text{Cl}_2\text{N}_4\text{SNi}$ ): C, 42.26; H, 3.04; N, 14.08;. Found: C, 43.16; H, 3.24; N, 14.10.

### 2.3. Synthesis of metal oxide nanoparticles from their corresponding complexes

50 mg of the different metal complexes were ground, placed in a ceramic crucible and calcined in the presence of air at 500°C with a heating rate of 10 °C min<sup>-1</sup> for 4 h to remove the organic contents. The samples were allowed to cool slowly to room temperature. The resulting nano-sized metal oxides were washed with ethanol and dried in air.

### 2.4. Crystal structure determination and refinement

Yellow block shaped crystals of Zn complexes and red needle shaped crystals of Ni complexes were obtained by slow diffusion of acetonitrile in DMF solution. A room temperature single-X-ray data collection was carried out on a Bruker Kappa Apex II, with Charge Coupled Device detector utilizing Mo-K $\alpha$  radiation. The data were collected by scanning  $\omega$  and  $\phi$  in different regions, with exposure times of 60 seconds per frame. The data were corrected for Lorentz and polarization effects using APEX II Suite Software, and absorption corrections were fitted

empirically using SADABS, since the crystal faces could not be determined reliably for numerical absorption corrections. The structure solutions were obtained by direct method and refined using the least square method incorporated into the SHELXTL package. All the non-hydrogen atoms were refined anisotropically and all the hydrogen atoms were refined in the idealized geometrically positions using a rigid model with C–H=0.93 Å, N–H=0.86 Å and isotropic displacement parameters  $U_{\text{iso}}(\text{H})=1.2U_{\text{eq}}(\text{C})$  for the aromatic ring and  $U_{\text{iso}}(\text{H})=1.5U_{\text{eq}}(\text{C})$  for the CH<sub>3</sub> group. A summary of crystal data, experimental details, and refinement results are given in Table 1.

< Table 1. >

## 2.5. Antibacterial assay

Antibacterial activity of Zn(II), Co(II) and Ni(II) thiosemicarbazone complexes and their corresponding metal oxide nanoparticles were tested in vitro using agar well diffusion method [28] against *Micrococcus luteus* (ATCC 4698), *Staphylococcus aureus* (ATCC 29213), *Bacillus subtilis* (DSM 6887), *Escherichia coli* (ATCC 25922) and *Pseudomonas aeruginosa* (ATCC 27853), supplied from the Iranian biological resource center, Tehran, Iran. The nutrient agar and nutrient broth cultures were prepared according to manufactures instructions and were incubated at 37°C. The nutrient agar plates were seeded with a suspension of 30µL of each bacterium after incubation for the appropriate time. Cups (0.5 cm in diameter) were cut in the agar using a sterilized glass tube. Then 30 µL of the test agents at a concentration of 1000 µg/ml in DMSO were introduced into each well. The plates were incubated at 37°C for 24 hrs. Clear zones around the wells showed the positive results and cloudiness indicates that bacterial growth has not been inhibited by the concentration of compound present in the medium. The diameter of inhibition zones was determined and values are expressed in millimeters (mm). The concentration of

DMSO in the medium did not affect the growth of any of the microorganisms tested. All experiments were made in triplicate to assess their reproducibility and the results were confirmed in three independent experiments. The results are reported as mean  $\pm$  standard deviation of zone of inhibition in millimeter. Antibacterial activity of each compound was compared with penicillin G and tetracycline as standard drugs. DMSO was used as a negative control.

### 3. Results and discussion

#### 3.1. General aspects

The thiosemicarbazone metal complexes were obtained by the reaction of corresponding metal salts and thiosemicarbazone ligand, in ethanolic solution. Experimental results showed that the thiosemicarbazone behaves as monoanionic ligand with deprotonation of hydrazine ( $N^2H$ ) proton. The infrared spectra of the thiosemicarbazone ligand and its metal complexes are shown in Fig. 1. A sharp and intense peak at  $1584\text{ cm}^{-1}$  on the FT-IR spectrum of HL can be assigned to  $\nu(C^8=N^3)$ . This band is shifted to lower frequencies in the spectra of the complexes (Table 2) which indicates the coordination of nitrogen to metal center [29]. Additionally, the bands at the  $3231\text{ cm}^{-1}$  and  $838\text{ cm}^{-1}$  in the IR spectrum of the free ligand, are corresponding to the  $\nu(N^2H)$  and  $\nu(C=S)$ , respectively. The attributed bands for  $N^2H$  and  $C=S$  vanished upon coordinating to the  $M^{2+}$  center (Table 2) suggesting the involvement of  $N^2$  and sulfur in coordination [30]. The new band at around  $1600\text{ cm}^{-1}$  for the metal complexes spectra can be attributed to stretching band of  $C^7=N^2$ . The metal ions are also bound by pyridine groups as evidenced by slightly shifting of the in-plane pyridine deformation bands to higher wavenumbers of complexes [31].

< Table 2. >

< Fig. 1.>

Fig. 2 shows the  $^1\text{H}$  NMR spectra of Zn(II) and Ni(II) complexes which were recorded in DMSO- $d_6$  solvent. The proton resonance for methyl group is found at  $\delta=3.32$  and 2.70 ppm for Ni(II) and Zn(II) complexes, respectively. The remarkable shift for  $\text{CH}_3$  moiety in complexes compared to HL ligand [27] suggests the involvement of the azomethine nitrogen in coordination to metal ions. Peaks of the aromatic protons of the p-chlorophenyl and pyridine groups were found in the region 7.33–8.26 ppm and 7.31-7.95 for Ni (II) and Zn(II) complexes, respectively. The signal arising from N(3)H moiety of HL at  $\delta=8.85$  [27] was not observed in  $^1\text{H}$  NMR spectra of the complexes. This observation proves that the ligand has undergone deprotonation before coordinating to metal center. The signals corresponding to N(1)H are observed at  $\delta=10.02$  and 9.42 ppm for Ni (II) and Zn(II) complexes, respectively. In addition, detection of only one set of signals in the  $^1\text{H}$  NMR spectrum of  $\text{ZnL}_2$  complex means that equivalent nuclei in the complexed ligand moieties are magnetically equivalent showing the same chemical shift. Residual solvent peaks for ethanol were seen at  $\delta=7.26$  and 2.50 ppm in  $^1\text{H}$  NMR spectrum of  $\text{ZnL}_2$  complex.

<Fig. 2>

The electronic spectral data for prepared thiosemicarbazone complexes in DMSO showed similar profiles which indicate the same mode of coordination of the thiosemicarbazone in complexes (Fig. 3). The high energy transitions were observed below 250 nm originate from  $\pi-\pi^*$  transitions associated with the aromatic rings in the ligands [32]. The bands recorded at the region 250-350 nm observed in the spectra of the ligand generally can be assigned to intra-ligand  $n\rightarrow\pi^*$  and  $\pi\rightarrow\pi^*$  transitions [33]. The synthesized metal complexes showed a characteristic absorption bands in the region 320–450 nm which is due to the charge transfer transition from HOMO of sulfur ( $\text{P}\pi$ -orbital) to the LUMO of metal ( $d\pi$ -orbital) [34].

< Fig. 3. >

### 3.2. Description of the molecular structures of $[\text{ZnL}_2]\cdot\text{CH}_3\text{CN}$ and $[\text{NiLCl}]$ complexes

#### 3.2.1. Structure of $[\text{ZnL}_2]\cdot\text{CH}_3\text{CN}$ complex

$[\text{ZnL}_2]\cdot\text{CH}_3\text{CN}$  crystallizes in the space group  $C2/c$ , with one Zn-atom and solvent molecule at special Wyckoff position 4e and the ligands at the general position 8f. The crystal structure consists of four crystallographically similar Zn(II) species in the asymmetric unit with a distorted octahedral geometry. Zn(II) ions are coordinated to two thiosemicarbazone ligands in their deprotonated form via the NNS donor atoms in a meridional fashion (Fig. 4). Selected bond lengths and angles with their standard deviations for  $[\text{ZnL}_2]\cdot\text{CH}_3\text{CN}$  complex are given in Table 3. The Zn–S and Zn–N(4) bond distances are 2.4632(8) Å and 2.244(2) Å, respectively and similar to those found in previous studies [35]. The Zn–N bond to the imine N-atom (2.147(2) Å) is shorter and of course stronger than that of pyridyl ring (2.244(2) Å) (Table 3). Given the fact that N(2) was deprotonated, the C–S bond is formally a single bond (1.725(3) Å) and the adjacent C(7)–N(2) bond (1.314(4) Å) was consistent with a tautomeric enol form. The bond lengths and angles for thiosemicarbazone coordination sites observed for  $[\text{ZnL}_2]\cdot\text{CH}_3\text{CN}$  are similar to previously reported 1:2 Zn(II)-thiosemicarbazone complexes in which the both ligands are deprotonated at the thioamide N-atom (N(2) in this structure) [2]. The molecules of  $[\text{ZnL}_2]\cdot\text{CH}_3\text{CN}$  complex are connected to each other by weaker hydrogen bonds N–H $\cdots$ S of 2.698 Å (Fig. 5).

< Table 3. >

< Fig. 4. >

<Fig.5>

#### 3.2.2. Structure of $[\text{NiLCl}]$ complex

[NiLCl] crystallizes in the space group  $C2/m$ , with all atoms at special Wyckoff position 4i except the H14B at the general position 8j. The asymmetric unit cell of the structure of [NiLCl] consists of four crystallographically dependent Ni(II) species. In this compound Ni(II) ion has four-coordination number in distorted square planar geometry, where the tridentate thiosemicarbazone ligand is deprotonated at N(2) atom. An ORTEP drawing of the asymmetric unit of [NiLCl] is presented in Fig. 6. Selected bond lengths and angles with their standard deviations for [NiLCl] are listed in Table 4. A notable feature is that the Ni-N(3) bond to the imine N-atom (1.857(3) Å) is much shorter than the bond to the pyridyl N-donor (1.920(3) Å) similar to that observed in [ZnL<sub>2</sub>].CH<sub>3</sub>CN complex. This lengthening of the Ni-N bond can be due to the trans influence of the Ni-Cl(2) bond. The Ni-S distance is 2.1548 Å which is a little shorter than those observed for [ZnL<sub>2</sub>].CH<sub>3</sub>CN but is within the range of those already reported in related Ni(II) complexes [36, 37]. In addition, the  $\pi$ - $\pi$  stacking between the (Cg(i)  $\rightarrow$  Cg(j)) interactions which form a 3D network have been presented in Fig. 7 and Table 5.

< Table 4.>

<Fig.6>

<Fig.7>

< Table 5.>

### 3.2.3. Proposed structure for Co(II) complex

As single crystals suitable for X-ray diffraction studies for the Co(II) complex of thiosemicarbazone ligand could not be obtained in different solvents, an attempt was conducted to determine the composition (metal to ligand ratio) of the complex by using Job's method [38]. The absorbance of each solution was then measured at  $\lambda=370$  nm and plotted vs. the volume

fraction of Ligand ( $V_L/(V_M + V_L)$ ), where  $V_M$  is the volume of the metal cation solution and  $V_L$  is the volume of the ligand solution. As shown in Fig. 8, the absorption at 370 nm increased as the volume fraction of the ligand increased matching the increased formation of the complex. The maximum absorbance occurs at ligand volume fraction of around 0.66, suggesting a complex of the formula  $ML_2$ .

< Fig. 8.>

In addition, mass spectrometric study of the Co(II) complex with thiosemicarbazone HL have been revealed a cation with  $m/z$  of 666.3 corresponding to the molecular mass of the structure of  $[CoL_2]^+$  ions (Fig. 9). The mass spectrum of this complex shows a large number of peaks assignable to various fragments arising from the thermal cleavage of the complex and ligand which suggest that the stoichiometry of the metal to ligand ratio to be 1:2 in the product. A schematic representation including the main fragmentation process for Co(II) complex is also given in Fig. 9.

< Fig. 9.>

In addition, on the basis of IR spectra, the deprotonated thiosemicarbazone ligands are bound to cobalt ion in a tridentate binding mode via the pyridine, sulfur and hydrazinic N donor atoms. Therefore, Co complex is expected to have a similar structure to that of complex  $[ZnL_2].CH_3CN$ . In addition, the similarity of UV-vis spectra between these two complexes suggests a distorted octahedral environment.

### 3.3. Synthesis and characterization of Zn, Co and Ni nano-sized metal oxides

In this work, the prepared thiosemicarbazone complexes have been used as precursors for the synthesis of their corresponding nano-sized metal oxides via thermal decomposition method and

are characterized by different spectroscopic methods. The typical powder XRD diffractograms of prepared metal oxides are given in Fig. 10. The observed XRD pattern for ZnO nanoparticles exhibited several well-defined diffraction peaks which are well-matched with the wurtzite hexagonal phase of pure ZnO [39]. All the diffraction peaks agreed with the reported 26170-ICSD standard data. The XRD result for NiO nanoparticles showed that the prepared solid is actually pure nickel oxide [40]. As can be seen, the XRD peaks positions are well matched with the reported 92131-ICSD standard data. The XRD results for  $\text{Co}_3\text{O}_4$  evidenced that the particles obtained were nanocrystalline and had a spinel structure [41]. All the Bragg peaks are consistent with those of the reported 56123-ICSD standard data. The average crystallite sizes were determined from the peak-width at half-height of the (101) peak for ZnO, the (200) peak for NiO and the (311) peak for  $\text{Co}_3\text{O}_4$  using the Debye-Scherrer equation:  $D = k\lambda/\beta\cos\theta$ , where, D is the average crystalline size, k the Scherrer constant (0.89),  $\lambda$  the X-ray wavelength used,  $\beta$  the angular line width of half maximum intensity and  $\theta$  is the Bragg's angle in degrees unit [42]. The calculated average crystallite sizes were found to be 41.6, 29.8 and 21.8 nm for ZnO, NiO, and  $\text{Co}_3\text{O}_4$ , respectively.

< Fig. 10. >

The morphologies of the nano metal oxides were determined by scanning electron microscope (SEM). The SEM images (Fig. 11) show that the obtained nanoparticles have similar morphologies and exhibit an approximately spherical shape. Moreover, the nanoparticles are of nano-dimensions in the size distributions ranged from of 20 nm to 40 nm which are consistent with the XRD analysis. Energy dispersive X-Ray (EDX) analyses of the synthesized metal oxides are presented in Fig. 11, which clearly demonstrated the presence of Zn, Ni and Co in the synthesized nanoparticles.

< Fig. 11. >

The FT-IR spectra of the oxides are shown in Fig. 12 which confirms the formation of nano-sized metal oxides via decomposition of thiosemicarbazone complexes. The spectra show absorption bands in the  $470 - 700 \text{ cm}^{-1}$  regions which assigned to the stretching vibration of the M-O bonds. The typical FT-IR measurements for  $\text{Co}_3\text{O}_4$  nanoparticles exhibit two absorption peaks at  $595 \text{ cm}^{-1}$  and  $677 \text{ cm}^{-1}$  which assigned to the stretching frequency of the metal-oxygen bonds in spinel compounds, respectively [43]. Strong bands around  $3500$  and  $1560 \text{ cm}^{-1}$  appeared in FT-IR spectra of the nanoparticles are attributed to the vibrational modes of O-H stretching and bending vibrations of surface hydroxyl groups and physisorbed water molecules. In the FT-IR spectra, all bands that were assigned to functional groups of the thiosemicarbazone complexes have been eliminated thus confirming the formation of the proposed pure and single phase of metal oxides.

<Fig.12>

### 3.4. Antimicrobial Activity

The newly synthesized thiosemicarbazone complexes and their corresponding nano-metal oxides were tested for their *in vitro* antibacterial activity against a series of gram positive and gram negative bacteria including *Micrococcus luteus* (*M. luteus*), *Staphylococcus aureus* (*S. aureus*), *Bacillus subtilis* (*B. subtilis*), *Escherichia coli* (*E. coli*) and *Pseudomonas aeruginosa* (*P. aeruginosa*), using the agar disc diffusion method. The antibacterial activity of tested agents was monitored at a concentration of  $1000 \mu\text{g/mL}$  in DMSO and the experiments were performed in triplicate. The trend in antimicrobial activity of the synthesized compounds was determined by measuring the inhibition zone in millimeters around the well and the results are presented as

mean  $\pm$  standard deviation in Table 6. Tetracycline and penicillin G were used as positive controls.

The comparison of the experimental results indicated that the complexation of thiosemicarbazone ligand affected its antimicrobial properties. Among the thiosemicarbazone complexes investigated in this work, [NiLCl] complex possessed a higher inhibition zone against *S. aureus* in comparison with its free ligand [27]. This finding confirmed that the antibacterial activity of thiosemicarbazone ligands can be enhanced by the metal center of the coordination compound [44]. However, [CoL<sub>2</sub>] complex was almost less active than HL against tested microorganisms, which is consistent with the previously reported cobalt cases [45]. In contrast to many reported Zn(II) complexes [46, 47], [ZnL<sub>2</sub>].CH<sub>3</sub>CN indicated lower antibacterial activity upon complexation with thiosemicarbazone ligand. However, this observation is similar to that of previously reported results for zinc(II) complexes with 4-ethyl-6-((E)-1-[(3-nitrophenyl)imino]ethyl)benzene-1,3-diol and 4-ethyl-6-((E)-1-[(2-nitrophenyl)imino]ethyl)benzene-1,3-diol Schiff-base ligands as presented by Nair et al. [48]. Bhaskar and coworkers showed that the complexes containing chloride ligand in their structure, possessed higher antibacterial activity [49]. Such results were also reported by Ruso et al. [50]. Therefore, in the light of the present observation, the higher antibacterial activity of [NiLCl] complex compared with [ZnL<sub>2</sub>].CH<sub>3</sub>CN and [CoL<sub>2</sub>] complexes may be attributed to the presence of chloride ligand in coordination sphere. This process may be either due to the lipophilic nature of the [NiLCl] complex, which favors their effective penetration through the lipid layer of the bacterial membrane cell [51]. On the contrary, the lower activity of the Co(II), and Zn(II) complexes can be attributed to the less ability of the complexes to permeate into the tested

microorganism membrane and thereby blocking their biological activity or they may diffuse and inactivated by unknown cellular mechanism such as bacterial enzymes [52, 53].

As shown in Table 6, [CoL<sub>2</sub>] and [NiLCl] complexes showed considerable inhibitory activity against the Gram-positive microorganisms tested and also *E. coli*. The cobalt oxide and zinc oxide nanoparticles effectively inhibited all tested aerobic Gram-positive strains and showed potential activity against Gram negative *E. coli* strain. Additionally, zones of bacterial growth inhibition of [NiLCl] complex and Co<sub>3</sub>O<sub>4</sub> was greater compared with other synthesized compounds in this study. All the compounds have no effect on Gram-negative bacteria, *P. aeruginosa* whereas they are moderately active for *E. coli* and Gram-positive strains. The activity of the Co<sub>3</sub>O<sub>4</sub> and ZnO were in the same range of the penicillin G against the *B. subtilis* and *E. coli*. The results indicate that the antimicrobial activity of nano-metal oxides is greater than that of their corresponding thiosemicarbazone complexes. Such increased activity of the metal oxides can be explained by the larger surface to volume ratio of nano-sized particles which results a more efficient antibacterial activities. Similar trends were reported previously [54].

<Table 6>

#### 4. Conclusions

Three new complexes of Zn(II), Ni(II) and Co(II) containing tridentate NNS-donor thiosemicarbazone have been prepared using ultrasonic irradiations and structurally characterized. The cobalt oxide, nickel oxide and zinc oxide nanoparticles were obtained by thermal decomposition of their respective thiosemicarbazone complex precursors at 500 °C. This method yields sphere-like metal oxide nanoparticles with weak agglomeration. The powder XRD patterns and EDX images of metal oxides indicate that pure and crystalline metal oxide phases are formed in all cases. Moreover, the nanostructures of metal oxides were further characterized

by SEM and FT-IR spectroscopy. All these compounds were further tested for antimicrobial activity against a series of gram positive and gram negative bacteria, using the zone inhibition methods and it was observed that the [NiLCl] complex was shown to possess more antimicrobial activity than its nano-sized metal oxide; however the prepared nano-sized zinc and cobalt oxides have been found to have the highest activity. The results of antimicrobial properties of thiosemicarbazone complexes and the nano-sized metal oxides presented in this study could be worthwhile to investigate the structure-bioactivity relationship of such compounds and elucidate the specific mechanisms involved in the antimicrobial action.

## 5. Supplementary material

The CIF files for crystal structure of [NiLCl] and [ZnL<sub>2</sub>]CH<sub>3</sub>CN complexes have been deposited with the CCDC No. 1587531 and 1587532, respectively. These data can be obtained free of charge from The Cambridge Crystallographic Data Centre via [www.ccdc.cam.ac.uk/data\\_request/cif](http://www.ccdc.cam.ac.uk/data_request/cif).

## Acknowledgements

The authors are grateful to the University of Guilan for financial support.

## References

- [1] N. Sampath, R. Mathews, M.N. Ponnuswamy, *J. Chem. Crystallogr.* 40 (2010) 1099–1104.
- [2] A.E. Stacy, D. Palanimuthu, P.V. Bernhardt, D.S. Kalinowski, P.J. Jansson, D.R. Richardson, *J. Med. Chem.* 59 (2016) 4965–4984.
- [3] A.I. Matesanz, , C. Hernández, and P. Souza, *J. Inorg. Biochem.* 138 (2014) 16–23.

- [4] S.M. Kumar, K. Dhahagani, J. Rajesh, K. Anitha, , G. Chakkaravarthi, N. Kanakachalam, M. Marappan, G. Rajagopal, *Polyhedron* 85 (2015) 830–840.
- [5] N. Sampath, R. Mathews, M.N. Ponnuswamy, L.W. Kang, *Mol. Cryst. Liq. Cryst.* 518 (2010) 151–159.
- [6] R. Ouyang, Y. Yang, X. Tong, Y. Yang, H. Tao, T. Zong, K. Feng, P. Jia, P. Cao, N. Guo, H. Chang, *Inorg. Chem. Commun.* 73 (2016) 138–141.
- [7] S.A. Khana, A.M. Asiri, *Int. J. Biol. Macromol.* 107 (2018) 105–111.
- [8] B.M. Zeglis, V. Divilov, J.S. Lewis, *J. Med. Chem.* 54 (2011) 2391–2398.
- [9] Y.Y. Wu, Y.T. Wang, Y.Y. Wang, M.X. Li, Y.L. Lu, Y.H. Zhang, *Inorg. Chem. Commun.* 78 (2017) 65–69.
- [10] Y. Gou, J. Wang, S. Chen, Z. Zhang, Y. Zhang, W. Zhang, F. Yang, *Eur. J. Med. Chem.* 123 (2016) 354–364.
- [11] A. MacGowan, E. Macnaughton, *Medicine* 41 (2013) 642–648.
- [12] J.H.B. Nunes, R.E.F. de Paiva, A. Cuin, A.M. da Costa Ferreira, W.R. Lustri, P.P. Corbi, *J. Mol. Struct.* 1112 (2016) 14–20.
- [13] T.S. Lobana, R. Sharma, G. Bawa, S. Khanna, *Coord. Chem. Rev.* 253 (2009) 977–1055.
- [14] J.R. Dilworth, R. Hueting, *Inorg. Chim. Acta*, 389 (2012) 3–15.
- [15] S. Shankar, J.W. Rhim, *Carbohydr. Polym.* 163 (2017) 137–145.
- [16] A. Sirelkhatim, S. Mahmud, A. Seenii, N.H.M. Kaus, L.C. Ann, S.K.M. Bakhori, H. Hasan, D. Mohamad, *Nano-Micro Lett.* 7 (2015) 219–242.
- [17] Y.Nassar, I.S.Ahmed, *Mater. Res. Bull.* 47 (2012) 2638 –2645.
- [18] M. Salavati-Niasari, A. Khansari, F. Davar, *Inorg. Chim. Acta* 362 (2009) 4937–4942.
- [19] M. Malathy, R. Jayasree, R. Rajavel, *Smart Sci.* (2017) 1–16.

- [20] M.Y. Nassar, A.S. Attia, K.A. Alfallous, M.F. El-Shahat, *Inorg. Chim. Acta* 405 (2013) 362–367.
- [21] M Salavati-Niasari, Z. Fereshteh, F. Davar, *Polyhedron* 28 (2009) 1065–1068.
- [22] S. Farhadi, K. Pourzare, S. Sadeghinejad, *J. Nanostructure Chem* 3 (2013) 16–22.
- [23] M.Y. Nassar, I.S. Ahmed, *Polyhedron* 30 (2011) 2431–2437.
- [24] F. Behnoudnia, H. Dehghani, *Polyhedron* 56 (2013) 102–108.
- [25] Z. Moradi-Shoeili, M. Zare, M. Bagherzadeh, M. Kubicki, D.M. Boghaei, *J. Coord. Chem.* 68 (2015) 548–559.
- [26] Z. Moradi-Shoeili, D. M. Boghaei, M. Amini, M. Bagherzadeh, B. Notash, *Inorg. Chem. Commun.* 27 (2013) 26–30.
- [27] Z. Piri, Z. Moradi-Shoeili, A. Assoud, *Inorg. Chem. Commun.* 84 (2017) 122–126.
- [28] N.O. Mahmoodi, S. Ramzanpour, F. Ghanbari Pirstasti, *Archiv. der Pharmazie.* 348 (2015) 275–282.
- [29] T.B.S.A. Ravoof, K.A. Crouse, E.R.T. Tiekink, M.I.M. Tahir, E.M. Yusof, R. Rosli, *Polyhedron* 133 (2017) 383–392.
- [30] D. Kovala-Demertzi, P.N. Yadav, J. Wiecek, S. Skoulika, T. Varadinova, M.A. Demertzis, *J. Inorg. Biochem.* 100 (2006) 1558–1567.
- [31] F. Bacher, E.A. Enyedy, N.V. Nagy, A. Rockenbauer, G.M. Bognár, R. Trondl, M.S. Novak, E. Klapproth, T. Kiss, V.B. Arion, , *Inorg. Chem.* 52 (2013) 8895–8908.
- [32] A. Bartyzel, H. Głuchowska, *J. Coord. Chem.* 69 (2016) 3206–3218.
- [33] T.S. Lobana, S. Indoria, H. Kaur, D.S. Arora, A.K. Jassal, J.P. Jasinski, *RSC Adv.* 5 (2015) 14916–14936.

- [34] D. Dayal, D. Palanimuthu, S.V. Shinde, K. Somasundaram, A.G. Samuelson, *J. Biol. Inorg. Chem.* 16 (2011) 621–632.
- [35] M.X. Li, C.L. Chen, D. Zhang, J.Y. Niu, B.S. Ji, *Eur. J. Med. Chem.* 45 (2010) 3169–3177.
- [36] R. Manikandan, P. Anitha, G. Prakash, P. Vijayan, P. Viswanathamurthi, *Polyhedron*, 81 (2014) 619–627.
- [37] S.R. Dinda, C.S. Schmiesing, E. Sinn, Y.P. Patil, M. Nethaji, H. Stoeckli-Evans, R. Acharyy, *Polyhedron* 50 (2013) 354–363.
- [38] E. Kouris, S. Kalogiannis, F. Perdih, I. Turel, G. Psomas, *J. Inorg. Biochem.* 163 (2016) 18–27.
- [39] M. Anbuvarannan, M. Ramesh, G. Viruthagiri, N. Shanmugam, N. Kannadasan, *Spectrochim. Acta A* 143 (2015) 304–308.
- [40] S. Rakshit, S. Ghosh, S. Chall, S.S. Mati, S.P. Moulik, S.C. Bhattacharya, *RSC Adv.* 3 (2013) 19348–19356.
- [41] L.S. Sundar, G.O. Irurueta, E.V. Ramana, M.K. Singh, A.C.M. Sousa, *Case Stud. Thermal Eng.* 7 (2016) 66–77.
- [42] B. D. Cullity, *Elements of X-Ray Diffraction*, Addison-Wesley, Reading, Mass, USA, 3rd edition, 1967.
- [43] M. Salavati-Niasari, A. Khansari, F. Davar, *Inorg. Chim. Acta*, 362 (2009) 4937–4942.
- [44] S.M. Alshehri, A. Al-Fawaz, F. Al-Ghamdi, T. Ahamad, *Adv. Polym. Tech.* 37(2018) 504–514.
- [45] L.A. Saghatforoush, F. Chalabian, A. Aminkhani, G. Karimnezhad, S. Ershad, *Eur. J. Med. Chem.* 44 (2009) 4490–4495.

- [46] S.M. Kumar, M.P. Kesavan, G.G.V. Kumar, M. Sankarganesh, G. Chakkaravarthi, G. Rajagopal, J. Rajesh, *J. Mol. Struct.* 1153 (2018) 1–11.
- [47] K. Singh, M.S. Barwa, P. Tyagi, *Eur. J. Med. Chem.* 42 (2007) 394–402.
- [48] R. Nair, A. Shah, S. Baluja, S. Chanda. *J. Serb. Chem. Soc.* 71(2006) 733–744.
- [49] R. Bhaskar, N. Salunkhe, A. Yaul, A. Aswar, *Spectrochim. Acta A*, 151 (2015) 621–627.
- [50] T. Rosu, E. Pahontu, C. Maxim, R. Georgescu, N. Stanica, Gabriela L. Almajan, A. Gulea, *Polyhedron* 29 (2010) 757–766.
- [51] Y.M. Zhao, G.M. Tang, Y.T.Wang, Y.Z. Cui, S.W. Ng, *J. Solid State Chem.* 259 (2018) 19–27.
- [52] T.A. Yousef, G.M.A. El-Reash, O.A. El-Gammal, R.A. Bedier, *J. Mol. Struct.* 1029 (2012) 149–160.
- [53] C. J. Dhanaraj, J. Johnson, *J. Coord. Chem.* 68 (2015) 2449–2469.
- [54] L.H. Abdel-Rahman, A.M. Abu-Dief, R.M. El-Khatib, S.M. Abdel-Fatah, *J. Photochem. Photobiol.* 162 (2016) 298–308.

Table 1. Crystallographic and structure refinement data for [ZnL<sub>2</sub>].CH<sub>3</sub>CN and [NiLCl] complexes.

	ZnL <sub>2</sub> .CH <sub>3</sub> CN	NiLCl
Empirical formula	C <sub>30</sub> H <sub>27</sub> Cl <sub>2</sub> N <sub>9</sub> S <sub>2</sub> Zn	C <sub>14</sub> H <sub>12</sub> Cl <sub>2</sub> N <sub>4</sub> NiS
Formula weight (g/mol)	713.99	397.95
Temperature (K)	296(2)	296(2)
Wavelength (Å)	0.71073	0.71073
Crystal system	monoclinic	monoclinic
Space group	<b>C2/c</b>	<b>C2/m</b>
Crystal size (mm <sup>3</sup> )	0.080×0.060×0.040	0.160×0.040×0.010
<i>a</i> (Å)	15.3056(3)	15.2299(4)
<i>b</i> (Å)	19.3414(4)	6.7241(2)
<i>c</i> (Å)	11.3234(2)	15.5196(4)
$\beta$ (°)	111.8808(10)	105.4872(16)
Volume (Å <sup>3</sup> )	3110.60(11)	1531.61(7)
Z	4	4
Calculated density (g cm <sup>-3</sup> )	1.525	1.726
$\theta$ Ranges for data collection (°)	1.5 - 30.0	1.5 - 30.0
F(000)	1464	808
Absorption coefficient (mm <sup>-1</sup> )	1.134	1.751
Index ranges	-20 ≤ <i>h</i> ≤ 20 -25 ≤ <i>k</i> ≤ 23 -14 ≤ <i>l</i> ≤ 6	-20 ≤ <i>h</i> ≤ 20 -8 ≤ <i>k</i> ≤ 7 -20 ≤ <i>l</i> ≤ 20
Number of Reflections	16167	13056
Unique data, ( <i>R</i> <sub>int</sub> )	856, (0.0707)	306, (0.0509)
Parameters / restraints	202 / 0	133 / 0
Final <i>R</i> <sub>1</sub> / <i>wR</i> <sub>2</sub> (obs. data)	0.0476 / 0.0834	0.0397 / 0.0620
Final <i>R</i> <sub>1</sub> / <i>wR</i> <sub>2</sub> (all data)	0.0921 / 0.0952	0.0781 / 0.0720
Goodness-of-fit on <i>F</i> <sup>2</sup> (S)	1.168	1.086
Largest diff. peak and hole (e Å <sup>-3</sup> )	0.377, -0.327	0.377, -0.499

Table 2. Infrared frequencies of the characteristic bands of the ligand and corresponding Zn(II), Ni(II) and Co(II) complexes.

Compound	$\nu(\text{N-H})$	$\nu(\text{C}^8=\text{N}^3)$	$\nu(\text{C}^7=\text{N}^2)$	$\nu(\text{C}^7=\text{S})$
HL	3231,3294	1584	–	832
[ZnL <sub>2</sub> ]	3363	1521	1591	781
[NiLCl]	3339	1536	1601	769
[CoL <sub>2</sub> ]	3338	1522	1603	767

Table 3. Selected bond distances (Å) and bond angles (°) for [ZnL<sub>2</sub>].CH<sub>3</sub>CN complex

Zn(1) N(3)	2.147(2) x2	Zn(1) N(4)	2.244(2)x2
Zn(1) S(1)	2.4632(8) x2	S(1) C(7)	1.725(3)
N(1) C(7)	1.376(3)	N(2) C(7)	1.314(4)
N(2) N(3)	1.375(3)	N(3) C(8)	1.291(3)
N(4) C(10)	1.335(3)	N(4) C(9)	1.342(3)
N(3) Zn(1) N(3)	165.05(12)	N(3) Zn(1) N(4)	73.43(8)
N(3) Zn(1) N(4)	95.23(8)	N(4) Zn(1) N(4)	83.56(12)
N(3) Zn(1) S(1)	111.59(6)	N(3) Zn(1) S(1)	78.64(6)
N(4) Zn(1) S(1)	95.67(6)	N(4) Zn(1) S(1)	151.85(6)
S(1) Zn(1) S(1)	97.79(4)	C(7) S(1) Zn(1)	95.56(9)
C(8) N(3) Zn(1)	120.03(18)	N(2) N(3) Zn(1)	123.65(17)
C(10) N(4) Zn(1)	127.1(2)	C(9) N(4) Zn(1)	114.73(17)
C(10) N(4) C(9)	118.2(3)	C(7) N(2) N(3)	113.4(2)

Table 4. Selected bond distances (Å) and bond angles (°) for [NiLCl].

Ni(1) N(3)	1.857(3)	Ni(1) N(4)	1.920(3)
Ni(1) S(1)	2.1548(11)	Ni(1) Cl(2)	2.1685(12)
S(1) C(7)	1.751(4)	N(1) C(7)	1.356(5)
N(1) C(1)	1.410(4)	N(2) C(7)	1.308(4)
N(2) N(3)	1.381(4)	N(3) C(8)	1.304(4)
N(4) C(10)	1.335(5)	N(4) C(9)	1.365(4)
N(3) Ni(1) N(4)	83.27(13)	N(3) Ni(1) S(1)	86.50(10)
N(4) Ni(1) S(1)	169.77(11)	N(3) Ni(1) Cl(2)	179.42(10)
N(4) Ni(1) Cl(2)	97.32(10)	S(1) Ni(1) Cl(2)	92.92(4)
C(7) S(1) Ni(1)	95.24(13)	C(8) N(3) Ni(1)	117.8(3)
N(2) N(3) Ni(1)	124.5(2)	C(9) N(4) Ni(1)	112.5(3)
C(10) N(4) Ni(1)	128.8(3)	C(7) N(2) N(3)	110.1(3)
C(10) N(4) C(9)	118.7(3)	C(8) N(3) N(2)	117.7(3)

Table 5. Stacking interactions, distances (Å) and angles (°).

Cg(i)···Cg(j)	d[Cg(i)···Cg(j)] <sup>a</sup>	d[Cg(i)···perp(j)] <sup>b</sup>	d[Cg(j)···perp(i)] <sup>c</sup>	$\alpha$	$\beta$	$\gamma$
Cg(1)···Cg(3) <sup>i</sup>	3.682(2)	-3.2358(13)	-3.3258(15)	3.82(16)	25.4	28.5
Cg(1)···Cg(3) <sup>ii</sup>	3.542 (2)	3.4973(13)	3.4591(15)	3.82(16)	12.5	9.1
Cg(2)···Cg(3) <sup>i</sup>	3.542 (2)	3.4591(15)	3.4974(13)	3.82(16)	9.1	12.5
Cg(2)···Cg(3) <sup>ii</sup>	3.682(2)	-3.3258(15)	-3.2357(13)	3.82(16)	28.5	25.4
Cg(3)···Cg(1) <sup>i</sup>	3.877(2)	3.4774(15)	3.4186(19)	4.1(2)	28.2	26.3
Cg(3)···Cg(2) <sup>i</sup>	3.878(2)	3.4187(19)	3.4774(15)	4.1(2)	26.3	28.2
Cg(3)···Cg(1) <sup>ii</sup>	3.878(2)	3.4187(19)	3.4774(15)	4.1(2)	26.3	28.2
Cg(3)···Cg(2) <sup>ii</sup>	3.878(2)	3.4187(19)	3.4774(15)	4.1(2)	26.3	28.2

Symmetry codes: (iii) =  $-4+x, 5/2-y, 1/2+z$ ; (iv) =  $-3+x, 5/2-y, 1/2+z$ .

a Distance between the centroids of ring i and ring j.

b Perpendicular distance from the centroid of ring i to ring j.

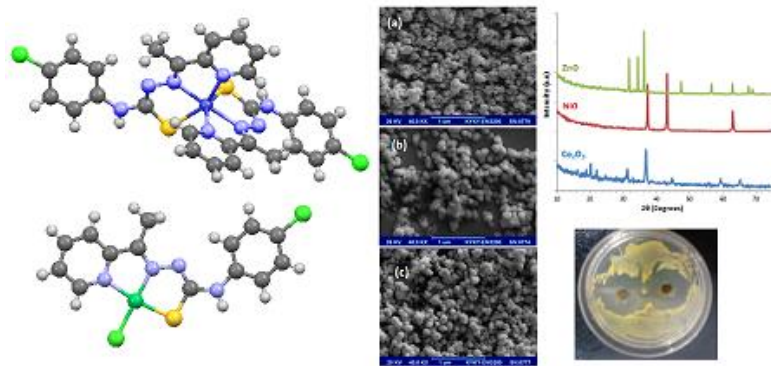
c Perpendicular distance from the centroid of ring j to ring i.

$\alpha$  = Dihedral angle between ring i and ring j(°);  $\beta$  = angle Cg(i)–Cg(j) vector and normal to plane i (°);  $\gamma$  = Angle Cg(i)–Cg(j) vector and normal to plane j (°). Cg(1) = centroid of ring [Cu1–O1–C11–C10–N2]; Cg(2) = centroid of ring [C1–C6] and Cg(3) = centroid of ring [C10–C15].

Table 6. Antibacterial activity of synthesized compounds and comparison to penicillin G and tetracycline as zone of inhibition (mm).

compounds	Antibacterial activity (mean±SD)				
	Gram Positive Bacteria			Gram Negative Bacteria	
	M. luteus	S. aureus	B. subtilis	E. coli	P. aeruginosa
<b>HL*</b>	20±1	12±1.0	15 ±1	12±1	10±1
<b>[CoL<sub>2</sub>]</b>	8 ±1	10 ±1	10 ± 1	8 ± 1	-
<b>[NiLCl]</b>	16 ±1	17± 1	9 ±1	7 ± 1	-
<b>[ZnL<sub>2</sub>]CH<sub>3</sub>CN</b>	-	-	6 ±1	-	-
<b>Co<sub>3</sub>O<sub>4</sub></b>	11±1	-	15±1	16± 1	-
<b>NiO</b>	-	-	15± 1	12±1	-
<b>ZnO</b>	14 ± 1	8 ± 1	10±1	14± 1	-
<b>Penicillin G</b>	50± 1	50±1	15± 1	18± 1	-
<b>Tetracycline</b>	46± 1	41± 1	31± 1	31± 1	27± 1

\*From [27]



ACCEPTED MANUSCRIPT

**Highlights:**

- Three new Zn(II), Co(II) and Ni(II) thiosemicarbazone complexes have been prepared using ultrasonic irradiations.
- Crystal structures and spectroscopic methods revealed distorted octahedral and/or square-planar coordination geometry around the central metals.
- The direct thermolysis of thiosemicarbazone complexes led to nano-sized metal oxides.
- The in vitro antibacterial activities were studied.

ACCEPTED MANUSCRIPT

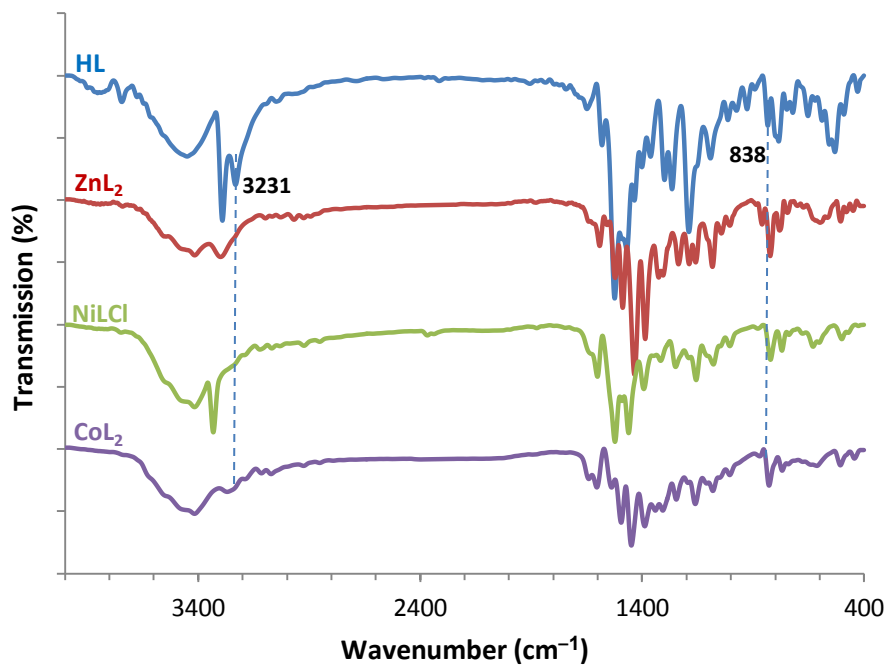


Fig. 1. FT-IR spectra of HL, [ZnL<sub>2</sub>].CH<sub>3</sub>CN, [CoL<sub>2</sub>] and [NiLCl] compounds.

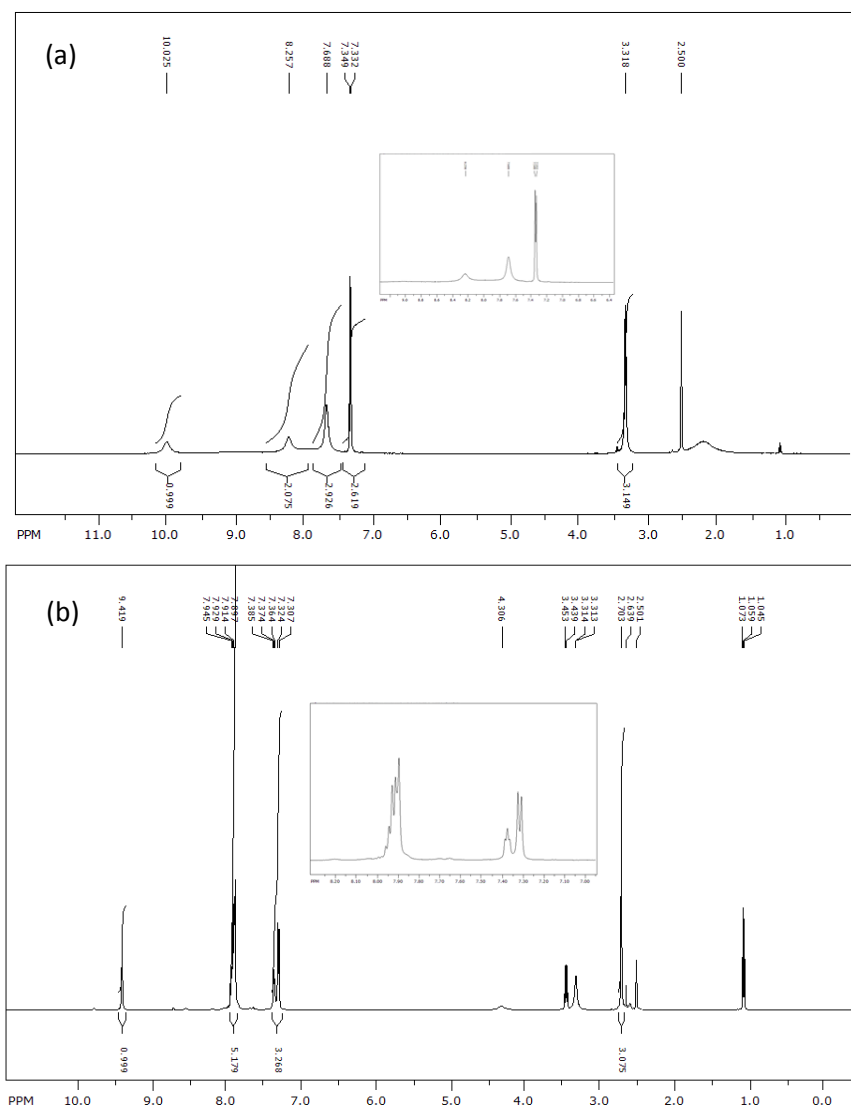


Fig. 2. The  $^1\text{H}$  NMR spectra of (a)  $\text{NiLCl}$  and (b)  $\text{ZnL}_2$  complexes. The insets show the expansion of aromatic region of complexes.

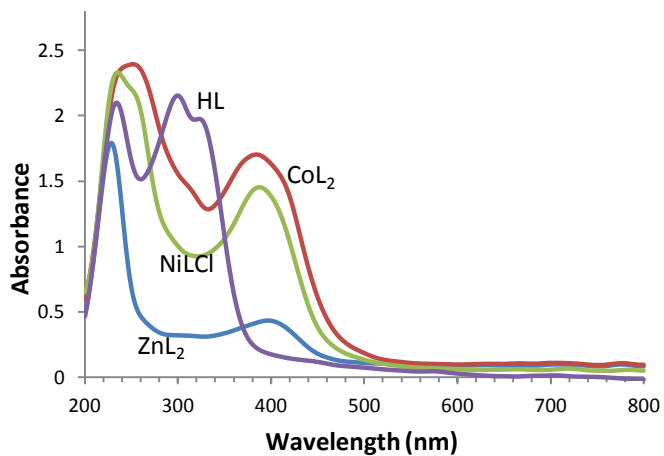


Fig. 3. UV-vis spectroscopy of ligand HL and corresponding Zn(II), Ni(II) and Co(II) complexes.

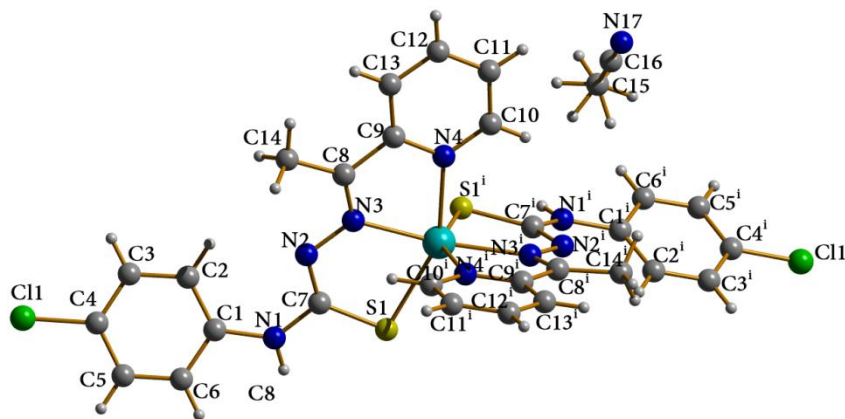


Fig. 4. Molecular structure of  $[\text{ZnL}_2]\cdot\text{CH}_3\text{CN}$  complex, showing the atom-labelling system and 50% thermal ellipsoids.

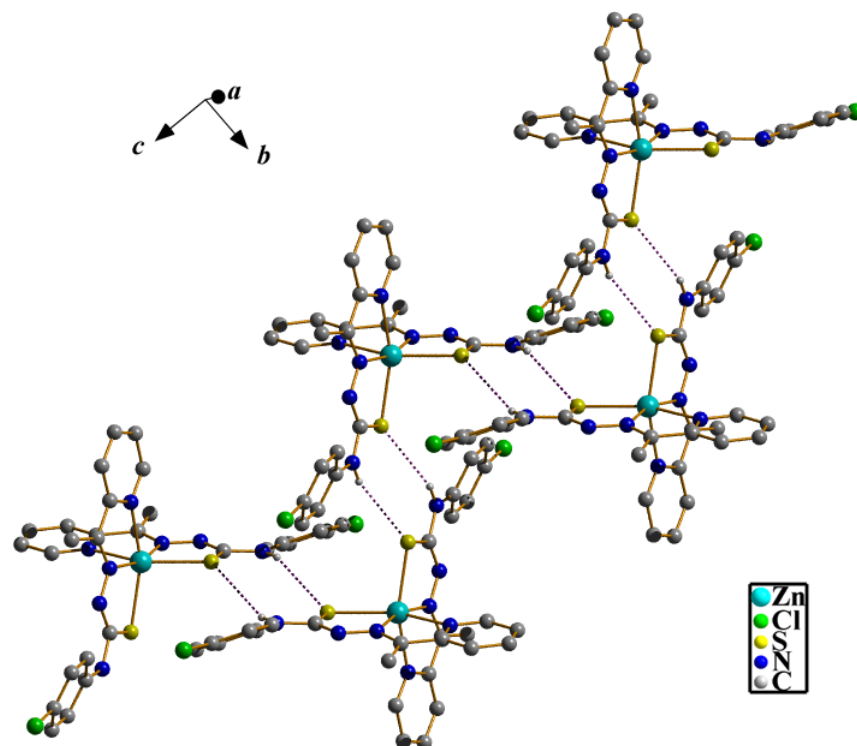


Fig. 5. Capped-stick representation of the packing of [ZnL<sub>2</sub>].CH<sub>3</sub>CN complex showing N-H...S hydrogen bonding (dash lines).

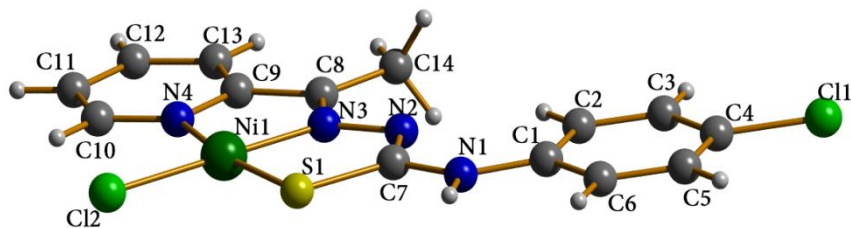


Fig. 6. Molecular structure of [NiLCl], showing the atom-labelling system and 50% thermal ellipsoids.

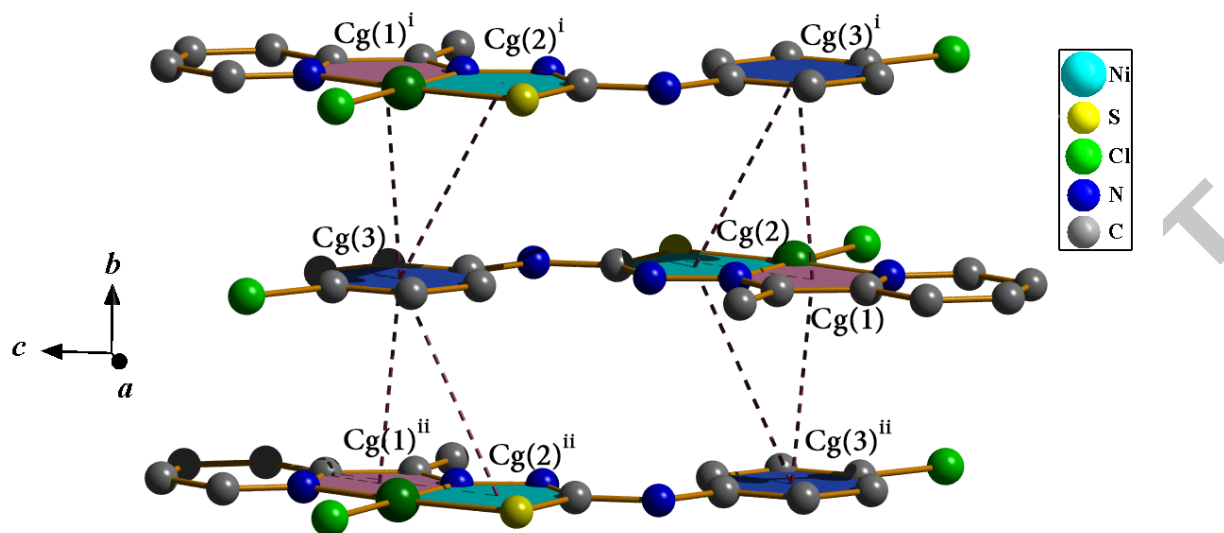


Fig. 7. The  $\pi$ - $\pi$  stacking between the  $Cg(i) \rightarrow Cg(j)$  interactions in [NiLCl] complex.

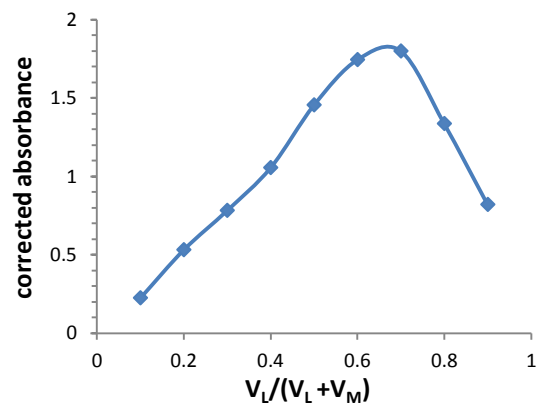


Fig. 8. Job's plot based on UV-Vis studies (at  $\lambda=370$  nm) for the prepared Co(II) complex in alcoholic solutions ( $[M] = [L] = 2.5 \times 10^{-4}$  M and  $T=298$  K).

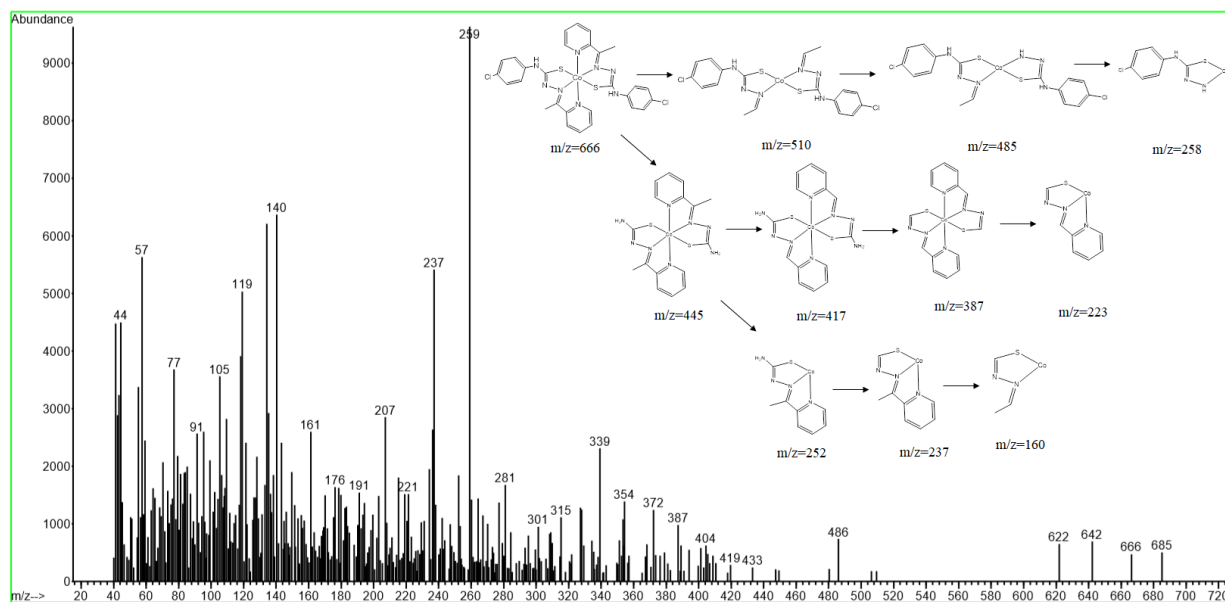


Fig. 9. Mass spectrum of the Co(II) complex. The inset shows the mass fragmentation routes of the metal complex.

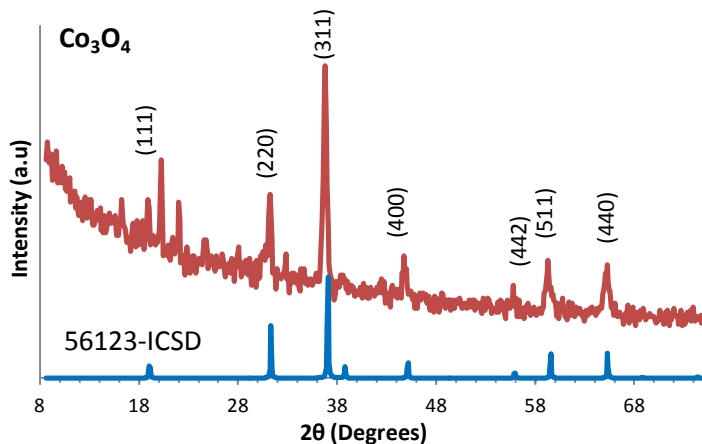
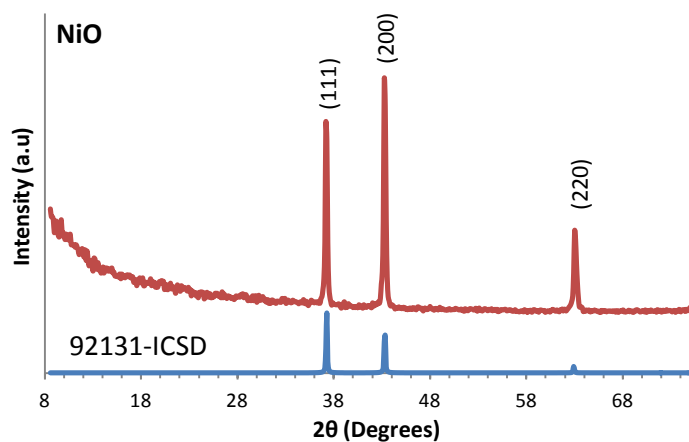
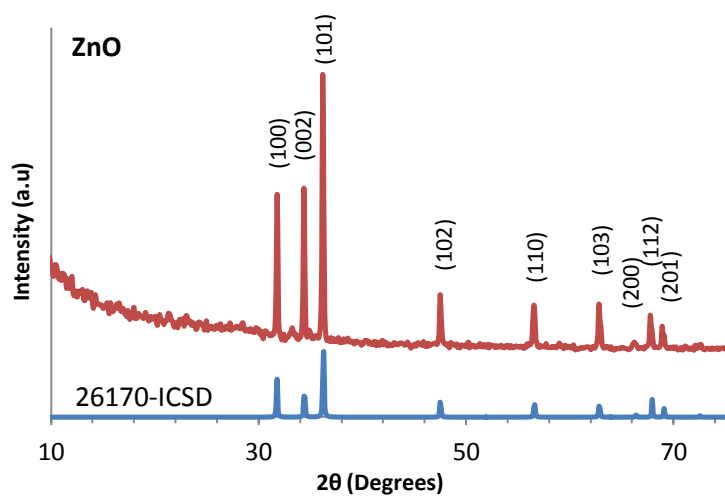


Fig. 10. XRD patterns of ZnO, NiO and Co<sub>3</sub>O<sub>4</sub> nanoparticles obtained by thermal decomposition. Standard XRD patterns are also presented for comparison.

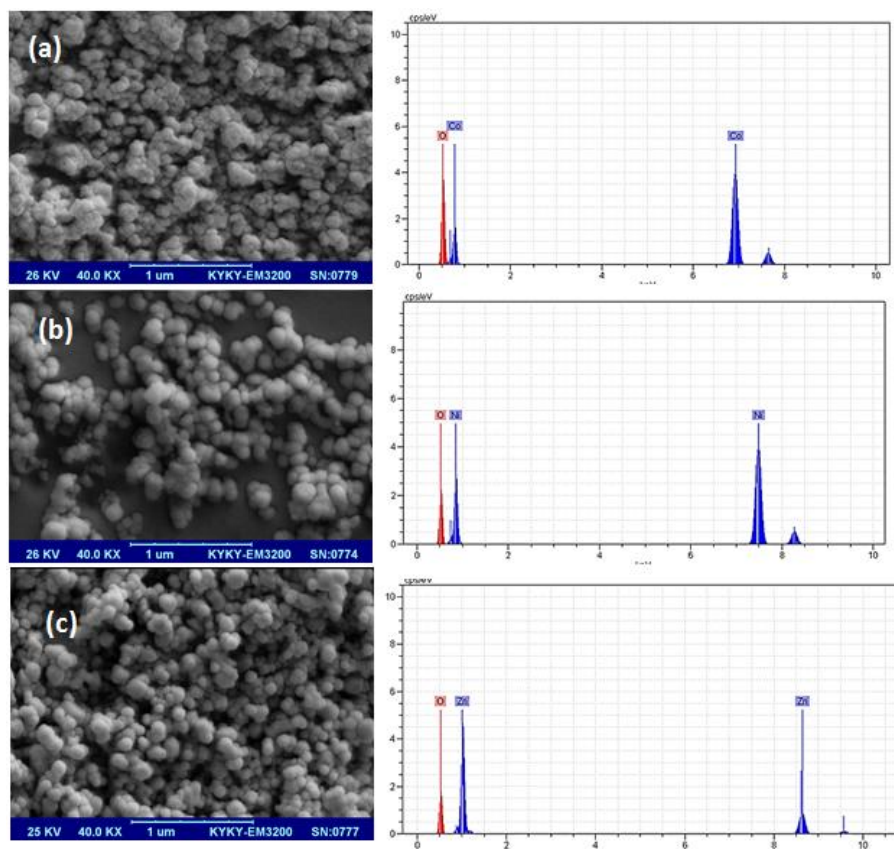


Fig. 11. SEM and EDX images of (a)  $\text{Co}_3\text{O}_4$  (b) NiO and (c) ZnO nanoparticles.

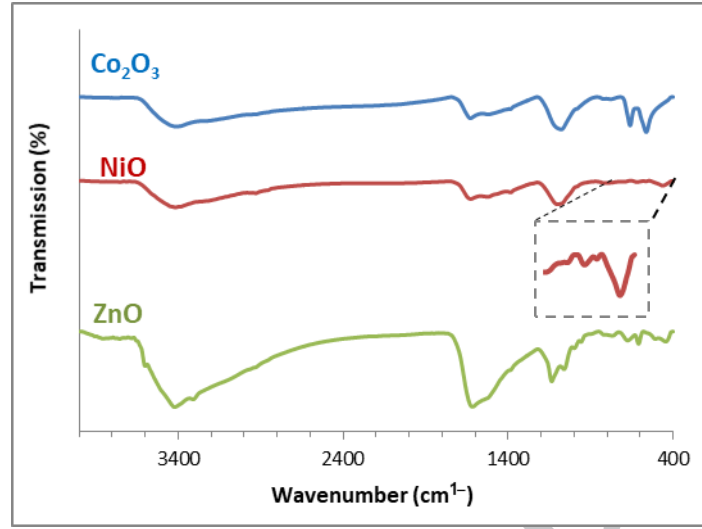


Fig. 12. The FT-IR spectra of the nano-metal oxides.